Supporting Information for:

Lightening Flavin by Amination for Fluorescent Sensing

Huimin Guo[1*], Siyu Liu[1], Xin Liu[1*] and Lijun Zhang[2]

[1]School of Chemistry, Dalian University of Technology, No. 2, Linggong Road, Dalian, 116024, P. R. China.

[2]Department of Ophthalmology, The Third People's Hospital of Dalian and Faculty of Medicine, Dalian University of Technology, No.2, Linggong Road, Dalian, 116024, P. R. China.

KEYWORDS:

Flavin; Fluorescent Emission; Intersystem Crossing; Photocatalysis; Isoalloxazine;

* Corresponding authors, email: guohm@dlut.edu.cn (H.G.) and xliu@dlut.edu.cn (X.L.)

Theoretical Methods

The electronic structure of AmFLs were investigated with extensive DFT and TD-DFT based calculations (Figure 1). Methyl was used to represent the alkyl moieties. The ground state (S_0) electronic structure of AmFLs were investigated at CAM-B3LYP/6−311G(d) level of theory.[1-4] Polarizable Continuum Model (PCM) was used to handle the impact of dichloromethane (DCM) solvent unless specified.[5-7] The electronic structures of excited AmFLs were investigated with TD-DFT based calculations at CAM-B3LYP/6−311G(d) level with Gaussian 16.[8] CAM-B3LYP function was selected as it can finely reproduce the ground state and excited state structures of heterocyclic and aromatic compounds obtained with second order coupled cluster method.[9] Similar combination of function and basis sets were used to interpret photophysical properties of FLs.[10-12] Frequency calculations were performed for all reported structures to insure there is no imagery frequencies and to obtain data for vibronic coupling analysis.

The transition dipole moments from T_1 to S_0 are evaluated from the quadratic response function[13-15] and the spin−orbit coupling matrix elements are computed at the same level of theory using the effective single-electron approximation in linear response theory with the Dalton program.[16-18]

The absorption, fluorescence and phosphorescence spectra of compounds, together with the radiative and non-radiative decay rate constants were calculated using MOMAP.[19-24] The absorption and fluorescence spectra were calculated according to eq-S1 and 2:

$$\sigma(\omega)_{abs} = \frac{4\pi^2\omega}{3\hbar c} \times \sum_{v_i,v_f} P_{iv_i}(T) \left|\left\langle \Theta_{f,v_f} \middle| \mu_{fi} \middle| \Theta_{i,v_i} \right\rangle\right|^2 \delta\left(\omega - \omega_{f,v_f,i,v_i}\right) \text{ (eq-S1)}$$

$$\sigma(\omega)_{emi} = \frac{4\omega^3}{3\hbar c} \times \sum_{v_i,v_f} P_{iv_i}(T) \left|\left\langle \Theta_{f,v_f} \middle| \mu_{fi} \middle| \Theta_{i,v_i} \right\rangle\right|^2 \delta\left(\omega_{i,v_i,f,v_f} - \omega\right) \text{(eq-S2)}$$

where $P_{iv_i}(T)$ is the Boltzmann population of the vibrational manifolds in the initial state, $\mu_{fi} = \langle \Phi_f | \mu | \Phi_i \rangle$ is the electronic transition dipole moment between the initial state i and final state f calculated according to the Frank-Condon approximation, v_i/v_f is vibrational quantum number of state i/f, Θ_{f,v_f} is the v_fth vibrational state of final state f, ω is the radiation frequency and $\omega_{i,v_i,f,v_f} = \omega_{f,v_f} - \omega_{i,v_i}$, respectively. The absorption and emission rate constants were calculated as the integration of the spectra.[24-27]

For the non-radiative decay, applying the second-order perturbation approximation, the rate constants were calculated as:

$$k_{f\leftarrow i} = \frac{2\pi}{\hbar} \sum_{v_i,v_f} P_{iv_i} \left| H'_{fv_f,iv_i} + \sum_{n,v_n} \frac{H'_{fv_f,nv_n} H'_{nv_n,iv_i}}{E_{iv_i} - E_{nv_n}} \right|^2 \times \delta\left(E_{iv_i} - E_{fv_f}\right) \text{ (eq-S3)}$$

where, v_i/v_f is vibrational quantum number of state i/f and H' is the interaction between 2 different Born-Oppenheimer states and calculated as $\mathrm{H}'\psi_{iv_i} = H^{NA}\Phi_i(r{:}Q)\Theta_{iv_i}(Q) + H^{SO}\Phi_i(r{:}Q)\Theta_{iv_i}(Q)$, where H^{NA} is the non-adiabatic coupling operator, H^{SO} is the spin-orbital coupling operator, r and Q are the electronic and nuclear normal mode coordinates.[28]

By applying a displayed oscillator mode and short time approximation, the internal conversion rate constant can be derived as:

$$log k_{ic,l}(\omega_{if}) \propto -\left(-\omega_{if} + \omega_i + \sum_{j(j\neq l)} S_j\omega_j\right)^2 / 2\sum_{j(j\neq l)} S_j {\omega_j}^2 (2n_j + 1) \text{(eq-S3')}$$

Where $S_j = \omega_j {D_j}^2/2\hbar$ is the Huang-Rhys factor and D_j is the displacement of *j*th mode, n_j is the phonon distribution function and $\lambda_j = S_j \hbar\omega_j$ is the reorganization of *j*th accepting mode.

By applying short-time approximation under the framework of the displaced harmonic oscillator model, the non-radiative decay rate constant for $T_1 \rightarrow S_0$ can be calculated as:

$$k'_{isc} = exp\left[-\frac{(\Delta E_{ad} - \sum_k \lambda_k)^2}{4\sum_k \lambda_k E_k} + ln\left(\frac{1}{\hbar}|\langle S_0|H^{SO}|T_1\rangle|^2\sqrt{\frac{\pi}{\sum_k \lambda_k E_k}}\right)\right] \text{(eq-S3'')}$$

Where ΔE_{ad} is the adiabatic excitation energy; $\lambda_k = S_k \hbar\omega_k = {\omega_k}^2 {D_k}^2/2$ is the reorganization energy for the *k*th mode; S_k and D_k are the Huang-Rhys factor and displacement of the mode with frequency of ω_k, respectively; E_k is the average vibration energy.

The transition dipole moment for phosphorescence was calculated as eq-S4:

$$\mu_{ST_\kappa} = \sum_k^{\{singlets\}} \frac{\langle S|\mu|\,{}^1k\rangle\langle\,{}^1k|H^{SO}|T_\kappa\rangle}{{}^3E_T^0 - {}^1E_k^0} + \sum_n^{\{triplets\}} \sum_{\kappa'=1}^{3} \frac{\langle S|H^{SO}|\,{}^3n_{\kappa'}\rangle\langle\,{}^3n_{\kappa'}|\mu|T_\kappa\rangle}{{}^1E_S^0 - {}^3E_n^0} \quad \text{(eq-S4)}$$

where κ is the magnetic quantum number, n and k are the intermediate triplet and singlet electronic states, respectively. Applying the Franck-Condon approximation, the phosphorescence spectra were calculated as eq-S5[23]:

$$\sigma_{ph}(\omega, T) = \frac{4\omega^3}{3\hbar c^3} \times \sum_{v_i, v_f} P_{iv_i}(T) \left|\left\langle \Theta_{f,v_f} \middle| \mu_{ST} \middle| \Theta_{i,v_i} \right\rangle\right|^2 \delta\left(\omega_{i,v_i,f,v_f} - \omega\right) \quad \text{(eq-S5)}$$

The radiative decay rate constant was calculated as the integration of the phosphorescence spectra.

The intersystem crossing rate constant can be calculated as:

$$k_{isc} = k_{isc}^{(0)} + k_{isc}^{(1)} + k_{isc}^{(2)} \quad \text{(eq-S6)}$$

where:

$$k_{isc}^{(0)} = \frac{2\pi}{\hbar}\sum_{v_i,v_f} P_{iv_i}\left|H'_{fv_f,iv_i}\right|^2 \times \delta\left(E_{iv_i} - E_{fv_f}\right) \text{ (eq-S7)}$$

$$k_{isc}^{(1)} = \frac{2\pi}{\hbar}\sum_{v_i,v_f} P_{iv_i} 2Re(H'_{fv_f,iv_i}\sum_{n,v_n}\frac{H'_{fv_f,nv_n}H'_{nv_n,iv_i}}{E_{iv_i}-E_{nv_n}}) \times \delta\left(E_{iv_i} - E_{fv_f}\right) \text{ (eq-S8)}$$

$$k_{isc}^{(2)} = \frac{2\pi}{\hbar}\sum_{v_i,v_f} P_{iv_i}\left|\sum_{n,v_n}\frac{H'_{fv_f,nv_n}H'_{nv_n,iv_i}}{E_{iv_i}-E_{nv_n}}\right|^2 \times \delta\left(E_{iv_i} - E_{fv_f}\right) \text{(eq-S9)}$$

Where H' is the interaction between 2 different Born-Oppenheimer states and calculated as $\mathrm{H}'\psi_{iv_i} = H^{NA}\Phi_i(r{:}\,Q)\Theta_{iv_i}(Q) + H^{SO}\Phi_i(r{:}\,Q)\Theta_{iv_i}(Q)$, where H^{NA} is the non-adiabatic coupling operator, H^{SO} is the spin-orbital coupling operator. More details on calculation of these spectra and rate constants can be found in Ref. 15-24.

The Simplified Kinetic Model

Based on the calculated photophysical properties and rate constants, the photophysical processes involved for evolution of FL and 8AmFL under continuous irradiation can be derived. They start with the population of FL and 8AmFL to spin allowed S_1. Then, the excited FL and 8AmFL would evolve via IC and FE from S_1. In absence of ICT for FL and 8AmFL, energy downhill ISC $S_1 \rightarrow T_n$ processes may also take place competing with IC and FE. After reaching T_n, excited FL and 8AmFL would decay into spin allowed T_1 very fast. Finally, these excited FL and 8AmFL at T_1 would decay via PE or nonradiative decay back to S_0.

The equations describing concentration of FL and 8AmFL at S_0, S_1, T_1, T_2 and T_3 as functions of time can be written as the following:

$$\frac{dc_{S_0}}{dt} = -k_{ad}c_{S_0} + c_{S_1}(k_f + k_{ic}) + \sum_1^n c_{T_n}\left[k_{p(T_n-S_0)} + k_{isc(T_n-S_0)}\right] \text{(eq-S10)}$$

$$\frac{dc_{S_1}}{dt} = k_{ad}c_{S_0} - c_{S_1}\left(k_f + k_{ic} + \sum_1^n k_{isc(S_1-T_n)}\right) + \sum_1^n c_{T_n}k_{RISC(T_n)} \text{(eq-S11)}$$

$$\frac{dc_{T_1}}{dt} = k_{isc(S_1-T_1)}c_{S_1} - c_{T_1}\left[k_{p(T_1)} + k_{isc(T_1-S_0)} + k_{RISC(T_1)}\right] + k_{ic(T_3-T_1)}c_{T_3} + k_{ic(T_2-T_1)}c_{T_2} \quad \text{(eq-S12)}$$

$$\frac{dc_{T_2}}{dt} = k_{isc(S_1-T_2)}c_{S_1} + k_{ic(T_3-T_2)}c_{T_3} - c_{T_2}\left[k_{p(T_2)} + k_{isc(T_2-S_0)} + k_{ic(T_2-T_1)} + k_{RISC(T_2)}\right] \text{(eq-S13)}$$

$$\frac{dc_{T_3}}{dt} = k_{isc(S_1-T_3)}c_{S_1} - c_{T_3}\left[k_{p(T_3)} + k_{isc(T_3-S_0)} + k_{ic(T_3-T_1)} + k_{ic(T_3-T_2)} + k_{RISC(T_3)}\right] \text{(eq-S14)}$$

Further to these,

$$k_{ad} = \sigma F \text{(eq-S15)}$$

$$F = \frac{P}{Ahv} = 6.79 \times 10^{19} \text{Photons} \cdot cm^{-2} \cdot s^{-1} \text{(eq-S16)}$$

$$10^{-\varepsilon cd} = e^{-\sigma nd} \text{(eq-S17)}$$

$$\sigma = \varepsilon \ln 10 \frac{c}{n} = \varepsilon\alpha = \alpha\varepsilon \text{(eq-S18)}$$

$$\alpha = 3.82 \times 10^{-21} mol \cdot cm^3 \cdot L^{-1} \text{(eq-S19)}$$

where σ is the absorption cross-section of sensitizer, P is the imput power of light radiation at 455 nm, that is 30 W, ε is the molecular extinction constant ($dm^3mol^{-1}cm^{-1}$), c is the concentration, in mol L^{-1}, n is the particle density, in cm^{-3}, d is path depth, in cm, α is the conversion constant, v is the frequency, A is the cross-section of light, that is 1 cm^2.

By solving equations Eq-S10 to Eq-S14 iteratively, with Eq-S16 to Eq-S19, calculated photophysical properties in Tables 1, 2 and 3, and assuming FL and 8AmFL are dissolved in dichloromethane solution of 0.033 mol/L at 298 K under continuous irradiation at wavelength of 455 nm, the steady state concentration of FL and 8AmFL at S_0, S_1, T_1, T_2 and T_3 can be obtained.

Table S1 Electronic transitions involved in the excitation of FL calculated at CAM-B3LYP/6-311G(d) level of theory.

	Energy	f[a]	Composition[b]	CI[c]	Character
$S_0 \rightarrow S_1$	3.4258 eV/361.91 nm	0.3385	59 → 60	0.69794	π→π*,n→π*
$S_0 \rightarrow S_2$	3.7314 eV/332.28 nm	0.0014	52 → 60	0.17627	n→π*
			56 → 60	0.49562	n→π*
			57 → 60	0.44861	n→π*
$S_0 \rightarrow S_3$	4.2272 eV/293.30 nm	0.0000	54 → 60	0.27741	n→π*
			54 → 63	0.10413	n→π*
			56 → 60	0.40692	n→π*
			57 → 60	0.44577	n→π*
			57 → 63	0.13391	n→π*
$S_0 \rightarrow S_4$	4.2905 eV/288.97 nm	0.1776	58 → 60	0.68343	π→π*,n→π*
			59 → 61	0.14822	π→π*,n→π*
$S_0 \rightarrow S_5$	5.0209 eV/246.94 nm	0.1173	53 → 60	0.23992	π→π*,n→π*
			55 → 60	0.48663	n→π*
			59 → 61	0.40244	π→π*,n→π*
$S_0 \rightarrow S_6$	5.0678 eV/244.65 nm	0.0001	52 → 60	0.29850	n→π*
			54 → 60	0.47776	n→π*
			56 → 60	0.20549	n→π*
			56 → 61	0.19740	n→π*
			56 → 65	0.10638	n→π*
			57 → 60	0.16024	n→π*
			57 → 61	0.12347	n→π*
$S_0 \rightarrow S_7$	5.2021 eV/238.33 nm	0.0001	52 → 60	0.50961	n→π*
			54 → 60	0.28077	n→π*
			56 → 61	0.19576	n→π*
			57 → 60	0.14898	n→π*
			57 → 61	0.21567	n→π*
$S_0 \rightarrow S_8$	5.3297 eV/232.63 nm	0.7328	55 → 60	0.4605	n→π*
			59 → 61	0.50447	π→π*,n→π*
$S_0 \rightarrow S_9$	5.4768 eV/226.38 nm	0.0223	53 → 60	0.44879	π→π*,n→π*
			55 → 60	0.16577	n→π*
			58 → 60	0.10048	π→π*,n→π*
			58 → 61	0.35326	π→π*,n→π*
			59 → 61	0.18744	π→π*,n→π*
			59 → 62	0.27446	π→π*,n→π*
$S_0 \rightarrow S_{10}$	5.9077 eV/209.87 nm	0.0612	53 → 60	0.46057	π→π*,n→π*
			53 → 62	0.10761	π→π*,n→π*
			58 → 61	0.26974	π→π*,n→π*
			59 → 62	0.41639	π→π*,n→π*
$S_0 \rightarrow T_1$	2.2932 eV/540.67 nm	0.0000	58 → 60	0.21460	π→π*,n→π*
			59 → 60	0.65825	π→π*,n→π*
$S_0 \rightarrow T_2$	2.8810 eV/430.35 nm	0.0000	58 → 60	0.56464	π→π*,n→π*

			58 → 62	0.21162	π→π*,n→π*
			59 → 60	0.21002	π→π*,n→π*
			59 → 61	0.24325	π→π*,n→π*
$S_0 \rightarrow T_3$	3.1258 eV/396.65 nm	0.0000	52 → 60	0.27122	n→π*
			56 → 60	0.47833	n→π*
			57 → 60	0.39553	n→π*
$S_0 \rightarrow T_4$	3.8959 eV/318.24 nm	0.0000	53 → 60	0.20230	π→π*,n→π*
			55 → 60	0.13346	n→π*
			58 → 60	0.26530	π→π*,n→π*
			59 → 61	0.57453	π→π*,n→π*
$S_0 \rightarrow T_5$	3.8988 eV/318.01 nm	0.0000	54 → 60	0.29867	n→π*
			54 → 63	0.14103	n→π*
			56 → 60	0.33699	n→π*
			57 → 60	0.45309	n→π*
			57 → 61	0.17204	n→π*

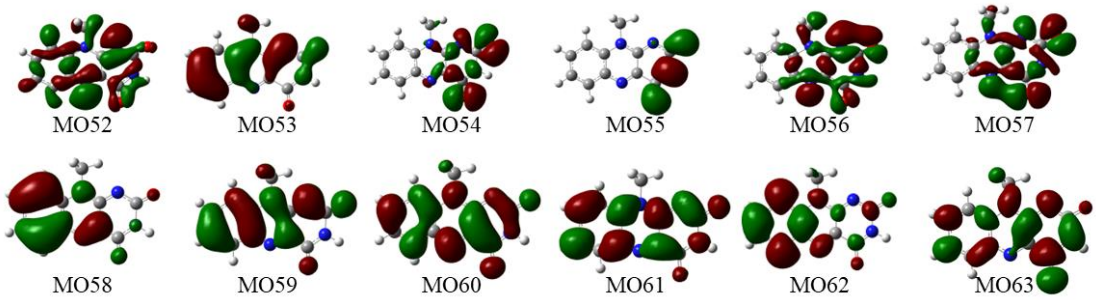

Figure S1. Isosurface plots of frontier molecular orbitals of FL involved in electron transitions contribute to UV-vis absorption obtained with calculations at CAM-B3LYP/6-311g(d) level of theory. (Isovalue: ±0.02 a.u.; C: Gray; O: Red; N: Blue; H: White.)

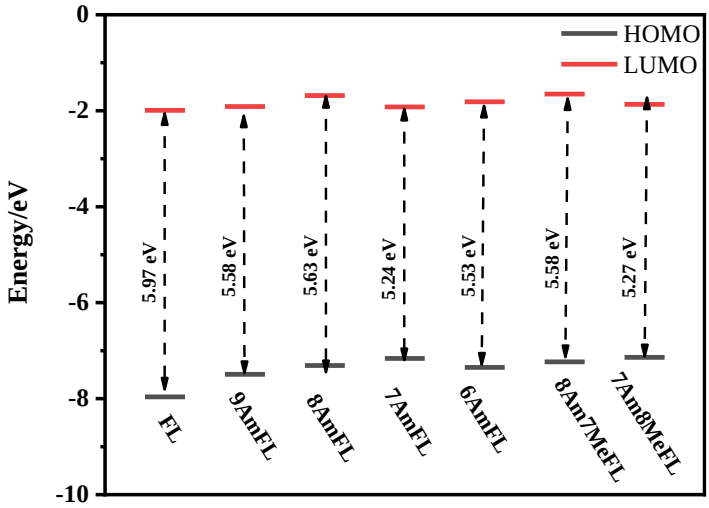

Figure S2. HOMO and LUMO of FL and AmFLs.

Table S2. Eigenvalues of HOMO and LUMO of FL and AmFLs.

Mol	E(HOMO)/eV	E(LUMO)/eV	ΔE/eV
FL	-7.96	-1.99	5.97
9AmFL	-7.49	-1.91	5.58
8AmFL	-7.31	-1.68	5.63
7AmFL	-7.16	-1.92	5.24
6AmFL	-7.35	-1.81	5.53
8Am7MeFL	-7.23	-1.65	5.58
7Am8MeFL	-7.14	-1.87	5.27

Table S3 Electronic transitions involved in the excitation of 6AmFL calculated at CAM-B3LYP/6-311G(d) level of theory.

	Energy	f	Composition	CI	Character
$S_0 \rightarrow S_1$	2.9733 eV/416.99 nm	0.1659	63 → 64	0.70225	n→π*
$S_0 \rightarrow S_2$	3.5179 eV/352.44 nm	0.3503	62 → 64	0.69493	n→π*
$S_0 \rightarrow S_3$	3.8932 eV/318.46 nm	0.0015	56 → 64	0.19485	n→π*
			60 → 64	0.58553	n→π*
			61 → 64	0.31220	n→π*
$S_0 \rightarrow S_4$	4.3393 eV/285.73 nm	0.0000	57 → 64	0.27834	n→π*
			60 → 64	0.28384	n→π*
			61 → 64	0.53171	n→π*
			61 → 66	0.10598	n→π*
			61 → 67	0.12296	n→π*
$S_0 \rightarrow S_5$	4.7470 eV/261.19 nm	0.2324	58 → 64	0.17236	π→π*,n→π*
			62 → 66	0.10394	π→π*,n→π*
			63 → 65	0.64404	π→π*,n→π*
			63 → 69	0.10244	π→π*,n→π*
$S_0 \rightarrow S_6$	5.0960 eV/243.30 nm	0.0259	58 → 64	0.18828	π→π*,n→π*
			59 → 64	0.43202	n→π*
			62 → 65	0.48245	π→π*,n→π*
			63 → 65	0.12086	π→π*,n→π*
$S_0 \rightarrow S_7$	5.1788 eV/239.41 nm	0.0001	56 → 64	0.26331	n→π*
			57 → 64	0.48541	n→π*
			60 → 64	0.15361	n→π*
			60 → 65	0.15998	n→π*
			61 → 64	0.20734	n→π*
			61 → 65	0.19820	n→π*
			61 → 69	0.12280	n→π*
$S_0 \rightarrow S_8$	5.3250 eV/232.83 nm	0.0002	56 → 64	0.51583	n→π*
			57 → 64	0.24533	n→π*
			60 → 65	0.27350	n→π*
			61 → 64	0.12019	n→π*
			61 → 65	0.16252	n→π*
$S_0 \rightarrow S_9$	5.4021 eV/229.51 nm	0.4613	59 → 64	0.51773	n→π*
			62 → 65	0.45090	π→π*,n→π*
$S_0 \rightarrow S_{10}$	5.6357 eV/220.00 nm	0.2962	58 → 64	0.64406	π→π*,n→π*
			59 → 64	0.13861	n→π*
			62 → 65	0.16816	π→π*,n→π*
			63 → 65	0.13413	π→π*,n→π*
$S_0 \rightarrow T_1$	2.0109 eV/616.56 nm	0.0000	62 → 64	0.36467	π→π*,n→π*
			63 → 64	0.58576	π→π*,n→π*
			63 → 66	0.11559	π→π*,n→π*
$S_0 \rightarrow T_2$	2.5144 eV/493.10 nm	0.0000	63 → 64	0.58507	π→π*,n→π*
			63 → 64	0.35119	π→π*,n→π*

$S_0 \rightarrow T_3$	3.2995 eV/375.77 nm	0.0000	56 → 64	0.29732	n→π*
			60 → 64	0.55426	n→π*
			61 → 64	0.25899	n→π*
$S_0 \rightarrow T_4$	3.6458 eV/340.08 nm	0.0000	58 → 64	0.18334	π→π*,n→π*
			62 → 65	0.42082	π→π*,n→π*
			63 → 65	0.41860	π→π*,n→π*
			63 → 66	0.17782	π→π*,n→π*
			63 → 67	0.18424	π→π*,n→π*
$S_0 \rightarrow T_5$	3.9154 eV/316.66 nm	0.0000	54 → 64	0.10261	n→π*
			58 → 64	0.29148	π→π*,n→π*
			59 → 64	0.13814	n→π*
			62 → 65	0.36636	π→π*,n→π*
			63 → 65	0.38647	π→π*,n→π*
			63 → 66	0.17947	π→π*,n→π*
			63 → 67	0.15624	π→π*,n→π*

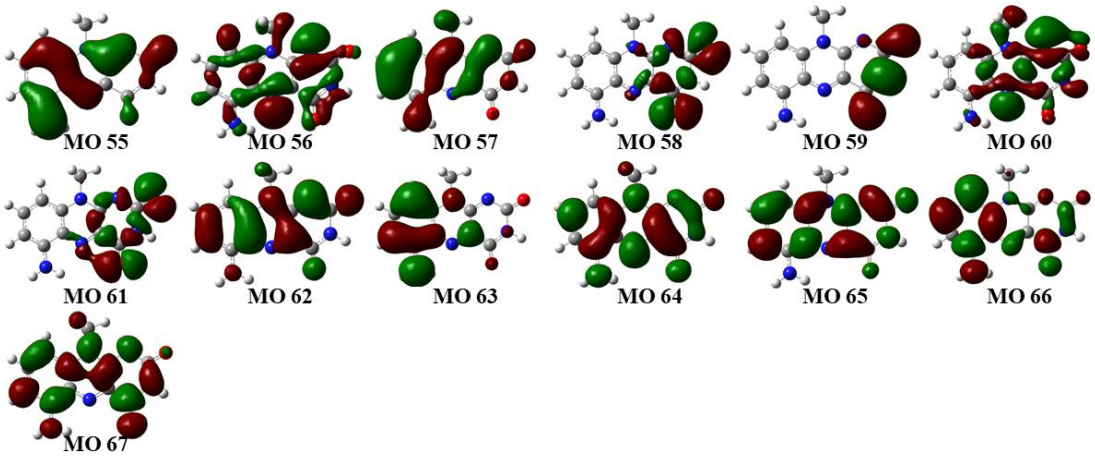

Figure S3. Isosurface plots of frontier molecular orbitals of 6AmFL involved in electron transitions contribute to UV-vis absorption obtained with calculations at CAM-B3LYP/6-311g(d) level of theory. (Isovalue: ±0.02 a.u.; C: Gray; O: Red; N: Blue; H: White.)

Table S4 Electronic transitions involved in the excitation of 7AmFL calculated at CAM-B3LYP/6-311G(d) level of theory.

	Energy	f	Composition	CI	Character
$S_0 \rightarrow S_1$	2.8720 eV/431.70 nm	0.2251	63 → 64	0.69944	π→π*,n→π*
$S_0 \rightarrow S_2$	3.7220 eV/333.11 nm	0.0014	56 → 64	0.18450	n→π*
			60 → 64	0.49029	n→π*
			61 → 64	0.45011	n→π*
$S_0 \rightarrow S_3$	4.1106 eV/301.62 nm	0.2457	62 → 64	0.68733	π→π*,n→π*
			63 → 65	0.11609	π→π*,n→π*
$S_0 \rightarrow S_4$	4.2393 eV/292.46 nm	0.0000	57 → 64	0.28776	n→π*
			60 → 64	0.40686	n→π*
			61 → 64	0.43796	n→π*
			61 → 67	0.12585	n→π*
$S_0 \rightarrow S_5$	4.6721 eV/265.37 nm	0.2036	58 → 64	0.20921	n→π*
			59 → 64	0.40419	π→π*,n→π*
			63 → 65	0.49948	π→π*,n→π*
			63 → 66	0.11405	π→π*,n→π*
$S_0 \rightarrow S_6$	5.0923 eV/243.47 nm	0.0509	56 → 64	0.32258	n→π*
			57 → 64	0.43981	n→π*
			59 → 64	0.15023	π→π*,n→π*
			60 → 64	0.20401	n→π*
			60 → 65	0.20161	n→π*
			61 → 64	0.15490	n→π*
			61 → 65	0.10913	n→π*
			63 → 65	0.11377	π→π*,n→π*
$S_0 \rightarrow S_7$	5.1079 eV/242.73 nm	0.7363	57 → 64	0.12607	n→π*
			59 → 64	0.49707	π→π*,n→π*
			63 → 65	0.42406	π→π*,n→π*
$S_0 \rightarrow S_8$	5.2092 eV/238.01 nm	0.0534	56 → 64	0.12387	n→π*
			58 → 64	0.55565	n→π*
			59 → 64	0.11243	π→π*,n→π*
			62 → 65	0.13810	π→π*,n→π*
			63 → 66	0.32357	π→π*,n→π*
$S_0 \rightarrow S_9$	5.2135 eV/237.81 nm	0.0021	56 → 64	0.48664	n→π*
			57 → 64	0.30237	n→π*
			58 → 64	0.13554	n→π*
			60 → 65	0.16447	n→π*
			61 → 64	0.16576	n→π*
			61 → 65	0.21180	n→π*
$S_0 \rightarrow S_{10}$	5.2907 eV/234.34 nm	0.1703	58 → 64	0.31530	n→π*
			59 → 64	0.18281	π→π*,n→π*
			62 → 65	0.13063	π→π*,n→π*
			63 → 65	0.10179	π→π*,n→π*
			63 → 66	0.55480	π→π*,n→π*

$S_0 \rightarrow T_1$	1.8667 eV/664.20 nm	0.0000	62 → 64	0.13942	π→π*,n→π*
			63 → 64	0.68384	π→π*,n→π*
			64 → 63	0.10284	n→π*
$S_0 \rightarrow T_2$	2.7162 eV/456.47 nm	0.0000	59 → 64	0.19705	π→π*,n→π*
			62 → 64	0.56987	π→π*,n→π*
			62 → 66	0.14376	π→π*,n→π*
			63 → 65	0.18811	π→π*,n→π*
			63 → 66	0.16661	π→π*,n→π*
$S_0 \rightarrow T_3$	3.1266 eV/396.55 nm	0.0000	56 → 64	0.27866	n→π*
			60 → 64	0.46958	n→π*
			61 → 64	0.40082	n→π*
$S_0 \rightarrow T_4$	3.4481 eV/359.57 nm	0.0000	59 → 64	0.29563	π→π*,n→π*
			62 → 64	0.27703	π→π*,n→π*
			63 → 65	0.52233	π→π*,n→π*
			63 → 66	0.10627	π→π*,n→π*
$S_0 \rightarrow T_5$	3.9164 eV/316.58 nm	0.0000	57 → 64	0.30987	n→π*
			57 → 67	0.13037	n→π*
			60 → 64	0.34186	n→π*
			61 → 64	0.44014	n→π*
			61 → 67	0.16193	n→π*

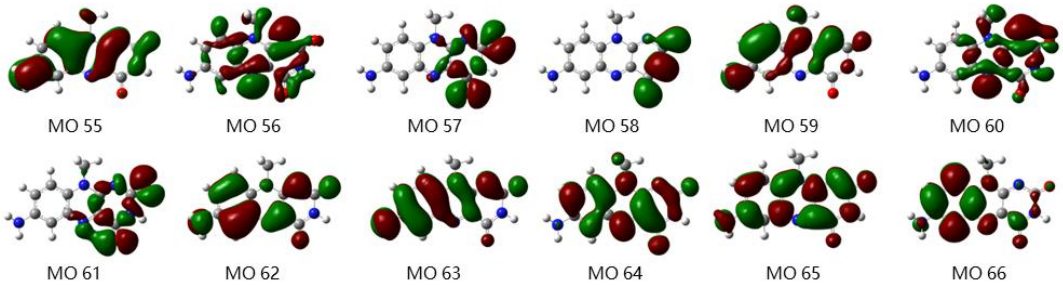

Figure S4. Isosurface plots of frontier molecular orbitals of 7AmFL involved in electron transitions contribute to UV-vis absorption calculated at CAM-B3LYP/6-311g(d) level of theory. (Isovalue: ±0.02 a.u.; C: Gray; O: Red; N: Blue; H: White.)

Table S5. Electronic transitions involved in the excitation of 8AmFL calculated at CAM-B3LYP/6-311G(d) level of theory.

	Energy	f	Composition	CI	Character
$S_0 \rightarrow S_1$	3.2766 eV/378.39 nm	0.7283	63 → 64	0.69231	π→π*,n→π*
$S_0 \rightarrow S_2$	3.9115 eV/316.97 nm	0.0016	56 → 64	0.19472	n→π*
			60 → 64	0.57858	n→π*
			61 → 64	0.32551	n→π*
$S_0 \rightarrow S_3$	3.9434 eV/314.41 nm	0.0197	62 → 64	0.68570	π→π*,n→π*
			63 → 65	0.10321	π→π*,n→π*
$S_0 \rightarrow S_4$	4.4070 eV/281.34 nm	0.0000	57 → 64	0.26345	n→π*
			57 → 67	0.10505	n→π*
			60 → 64	0.29335	n→π*
			61 → 64	0.53054	n→π*
			61 → 67	0.15763	n→π*
$S_0 \rightarrow S_5$	4.8349 eV/256.43 nm	0.1062	58 → 64	0.16234	π→π*,n→π*
			62 → 64	0.13305	π→π*,n→π*
			63 → 65	0.63486	π→π*,n→π*
			63 → 66	0.16761	π→π*,n→π*
$S_0 \rightarrow S_6$	5.1643 eV/240.08 nm	0.0853	55 → 64	0.10971	π→π*,n→π*
			58 → 64	0.34582	π→π*,n→π*
			59 → 64	0.40251	n→π*
			62 → 65	0.33013	π→π*,n→π*
			63 → 65	0.14447	π→π*,n→π*
			63 → 66	0.23182	π→π*,n→π*
$S_0 \rightarrow S_7$	5.2253 eV/237.28 nm	0.0001	56 → 64	0.29927	n→π*
			57 → 64	0.46495	n→π*
			57 → 67	0.10608	n→π*
			60 → 64	0.17243	n→π*
			60 → 65	0.18416	n→π*
			61 → 64	0.17867	n→π*
			61 → 65	0.16731	n→π*
			61 → 69	0.10288	n→π*
$S_0 \rightarrow S_8$	5.3638 eV/231.15 nm	0.0001	56 → 64	0.48800	n→π*
			57 → 64	0.27733	n→π*
			60 → 65	0.24406	n→π*
			61 → 64	0.13922	n→π*
			61 → 65	0.19246	n→π*
$S_0 \rightarrow S_9$	5.4865 eV/225.98 nm	0.3800	59 → 64	0.52545	n→π*
			62 → 65	0.32282	π→π*,n→π*
			63 → 65	0.15943	π→π*,n→π*
			63 → 66	0.27038	π→π*,n→π*
$S_0 \rightarrow S_{10}$	5.6499 eV/219.44 nm	0.1234	58 → 64	0.56502	π→π*,n→π*
			59 → 64	0.19872	n→π*
			62 → 65	0.20939	π→π*,n→π*

			63 → 66	0.25646	π→π*,n→π*
$S_0 \rightarrow T_1$	2.0122 eV/616.16 nm	0.0000	63 → 64	0.69726	π→π*,n→π*
			64 → 63	0.12141	π*→π,π*→n
$S_0 \rightarrow T_2$	2.9517 eV/420.05 nm	0.0000	58 → 66	0.10349	π→π*,n→π*
			62 → 64	0.61238	π→π*,n→π*
			63 → 65	0.26003	π→π*,n→π*
			63 → 66	0.10087	π→π*,n→π*
$S_0 \rightarrow T_3$	3.2743 eV/378.66 nm	0.0000	56 → 64	0.29182	n→π*
			60 → 64	0.54605	n→π*
			61 → 64	0.27628	n→π*
$S_0 \rightarrow T_4$	3.9121 eV/316.92 nm	0.0000	58 → 64	0.18194	π→π*,n→π*
			58 → 66	0.10352	π→π*,n→π*
			59 → 64	0.11560	π→π*,n→π*
			62 → 64	0.28701	π→π*,n→π*
			62 → 65	0.16775	π→π*,n→π*
			63 → 65	0.52389	π→π*,n→π*
			63 → 66	0.10329	π→π*,n→π*
$S_0 \rightarrow T_5$	4.0594 eV/305.42 nm	0.0000	58 → 64	0.51767	π→π*,n→π*
			58 → 65	0.12344	π→π*,n→π*
			58 → 66	0.13733	π→π*,n→π*
			62 → 66	0.16772	π→π*,n→π*
			63 → 65	0.26780	π→π*,n→π*
			63 → 66	0.24731	π→π*,n→π*

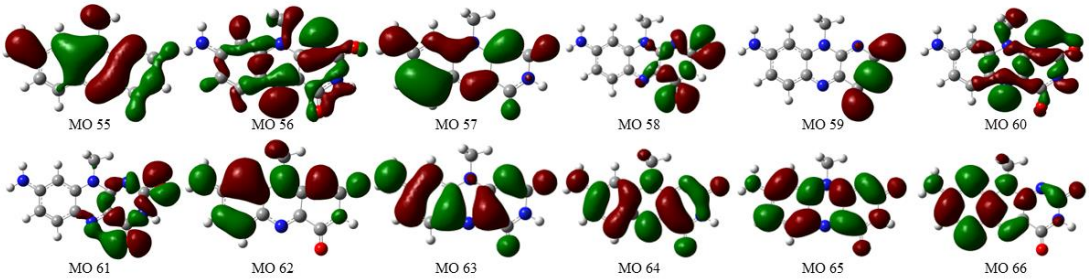

Figure S5. Isosurface plots of frontier molecular orbitals of 8AmFL involved in electron transitions contribute to UV-vis absorption. (Isovalue: ±0.02 a.u.; C: Gray; O: Red; N: Blue; H: White.)

Table S6. Electronic transitions involved in the excitation of 9AmFL calculated at CAM-B3LYP/6-311G(d) level of theory.

	Energy	f	Composition	CI	Character
$S_0 \rightarrow S_1$	3.1075 eV/398.99 nm	0.0666	63 → 64	0.69645	π→π*,n→π*
$S_0 \rightarrow S_2$	3.7058 eV/334.57 nm	0.2258	55 → 64	0.11586	n→π*
			60 → 64	0.24309	n→π*
			61 → 64	0.35297	n→π*
			62 → 64	0.52836	π→π*,n→π*
$S_0 \rightarrow S_3$	3.7337 eV/332.07 nm	0.1658	55 → 64	0.11856	n→π*
			60 → 64	0.31136	n→π*
			61 → 64	0.41117	n→π*
			62 → 64	0.43983	π→π*,n→π*
$S_0 \rightarrow S_4$	4.2475 eV/291.90 nm	0.0012	58 → 64	0.27463	n→π*
			58 → 67	0.10767	n→π*
			60 → 64	0.49045	n→π*
			61 → 64	0.35421	n→π*
			61 → 67	0.12882	n→π*
$S_0 \rightarrow S_5$	4.6951 eV/264.07 nm	0.4470	57 → 64	0.15711	π→π*,n→π*
			59 → 64	0.13781	n→π*
			62 → 66	0.13877	π→π*,n→π*
			63 → 65	0.63550	π→π*,n→π*
$S_0 \rightarrow S_6$	5.0743 eV/244.34 nm	0.0006	55 → 64	0.27986	n→π*
			56 → 64	0.12766	π→π*,n→π*
			58 → 64	0.47170	n→π*
			60 → 64	0.22603	n→π*
			60 → 65	0.21688	n→π*
			60 → 69	0.11519	n→π*
			61 → 64	0.11581	n→π*
$S_0 \rightarrow S_7$	5.1724 eV/239.71 nm	0.0972	59 → 64	0.61288	n→π*
			62 → 65	0.24247	π→π*,n→π*
			63 → 65	0.14090	π→π*,n→π*
$S_0 \rightarrow S_8$	5.2054 eV/238.18 nm	0.0039	55 → 64	0.47518	n→π*
			56 → 64	0.17343	π→π*,n→π*
			58 → 64	0.28762	n→π*
			60 → 65	0.14999	n→π*
			61 → 64	0.14892	n→π*
			61 → 65	0.25042	n→π*
$S_0 \rightarrow S_9$	5.4032 eV/229.46 nm	0.2536	57 → 64	0.21505	π→π*,n→π*
			59 → 64	0.19342	n→π*
			62 → 65	0.57361	π→π*,n→π*
			63 → 65	0.11863	π→π*,n→π*
			63 → 66	0.18176	π→π*,n→π*
$S_0 \rightarrow S_{10}$	5.7085 eV/217.19 nm	0.0260	57 → 64	0.55911	π→π*,n→π*
			59 → 64	0.15976	n→π*

			63 → 65	0.11443	π→π*,n→π*
			63 → 66	0.31698	π→π*,n→π*
$S_0 \rightarrow T_1$	2.2039 eV/562.56 nm	0.0000	62 → 64	0.22565	π→π*,n→π*
			63 → 64	0.64860	π→π*,n→π*
$S_0 \rightarrow T_2$	2.3871 eV/519.39 nm	0.0000	56 → 64	0.15134	π→π*,n→π*
			62 → 64	0.61571	π→π*,n→π*
			62 → 65	0.10044	π→π*,n→π*
			63 → 64	0.17490	π→π*,n→π*
			63 → 66	0.18737	π→π*,n→π*
			64 → 62	0.10033	*π→π,π*→n
$S_0 \rightarrow T_3$	3.1181 eV/397.63 nm	0.0000	55 → 64	0.25875	n→π*
			60 → 64	0.38599	n→π*
			61 → 64	0.49090	n→π*
$S_0 \rightarrow T_4$	3.5479 eV/349.45 nm	0.0000	57 → 64	0.13092	π→π*,n→π*
			62 → 64	0.13027	π→π*,n→π*
			62 → 65	0.21296	π→π*,n→π*
			62 → 66	0.10040	π→π*,n→π*
			63 → 64	0.10401	π→π*,n→π*
			63 → 65	0.56751	π→π*,n→π*
			63 → 66	0.18742	π→π*,n→π*
$S_0 \rightarrow T_5$	3.9124 eV/316.90 nm	0.0000	58 → 64	0.29835	n→π*
			58 → 67	0.14409	n→π*
			60 → 64	0.42652	n→π*
			61 → 64	0.37037	n→π*
			61 → 67	0.16338	n→π*

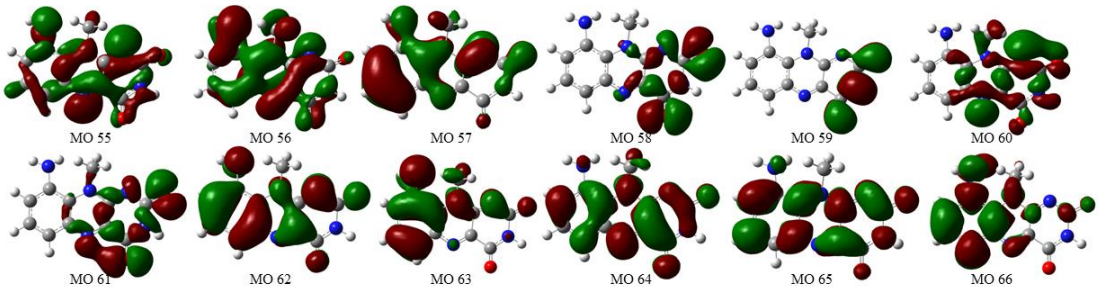

Figure S6. Isosurface plots of frontier molecular orbitals of 9AmFL involved in electron transitions contribute to UV-vis absorption. (Isovalue: ±0.02 a.u.; C: Gray; O: Red; N: Blue; H: White.)

Table S7. Electronic transitions involved in the excitation of 8Am7MeFL.

	Energy	f	Composition	CI	Character
$S_0 \rightarrow S_1$	3.2394 eV/382.74 nm	0.7426	67 → 68	0.69302	π→π*,n→π*
$S_0 \rightarrow S_2$	3.8912 eV/318.63 nm	0.0297	66 → 68	0.68722	π→π*,n→π*
$S_0 \rightarrow S_3$	3.9185 eV/316.41 nm	0.0015	60 → 64	0.19612	n→π*
			64 → 68	0.58287	n→π*
			65 → 68	0.31665	n→π*
$S_0 \rightarrow S_4$	4.4177 eV/280.66 nm	0.0000	61 → 68	0.26579	n→π*
			61 → 71	0.10537	n→π*
			64 → 68	0.28491	n→π*
			65 → 68	0.53372	n→π*
			65 → 71	0.15617	n→π*
$S_0 \rightarrow S_5$	4.8673 eV/254.73 nm	0.1409	62 → 68	0.16255	π→π*,n→π*
			66 → 68	0.13068	π→π*,n→π*
			67 → 69	0.63163	π→π*,n→π*
			67 → 70	0.15890	π→π*,n→π*
$S_0 \rightarrow S_6$	5.1173 eV/242.28 nm	0.0874	59 → 67	0.10201	n→π*
			62 → 68	0.49994	π→π*,n→π*
			63 → 68	0.22655	π→π*,n→π*
			66 → 69	0.30017	π→π*,n→π*
			67 → 69	0.16900	π→π*,n→π*
			67 → 70	0.22156	π→π*,n→π*
$S_0 \rightarrow S_7$	5.2400 eV/236.61 nm	0.0000	60 → 68	0.30609	n→π*
			61 → 68	0.45961	n→π*
			61 → 71	0.10333	n→π*
			64 → 68	0.17308	n→π*
			64 → 69	0.18842	n→π*
			65 → 68	0.18101	n→π*
			65 → 69	0.16991	n→π*
			65 → 74	0.10580	n→π*
$S_0 \rightarrow S_8$	5.3768 eV/230.59 nm	0.0001	60 → 68	0.48435	n→π*
			61 → 68	0.28348	n→π*
			64 → 69	0.24410	n→π*
			65 → 68	0.14261	n→π*
			65 → 69	0.19491	n→π*
$S_0 \rightarrow S_9$	5.4774 eV/226.35 nm	0.3441	63 → 68	0.56216	π→π*,n→π*
			66 → 69	0.26574	π→π*,n→π*
			67 → 69	0.16034	π→π*,n→π*
			67 → 70	0.24913	π→π*,n→π*
$S_0 \rightarrow S_{10}$	5.5531 eV/223.27 nm	0.1288	62 → 68	0.43762	π→π*,n→π*
			63 → 68	0.31815	π→π*,n→π*
			66 → 69	0.27523	π→π*,n→π*
			67 → 70	0.32113	π→π*,n→π*
$S_0 \rightarrow T_1$	1.9839 eV/624.94 nm	0.0000	67 → 68	0.69850	π→π*,n→π*

			68 → 67	0.12287	n→π*
$S_0 \rightarrow T_2$	2.8987 eV/427.73 nm	0.0000	62 → 70	0.10113	π→π*,n→π*
			66 → 68	0.61584	π→π*,n→π*
			67 → 69	0.25800	π→π*,n→π*
$S_0 \rightarrow T_3$	3.2816 eV/377.81 nm	0.0000	60 → 68	0.29231	n→π*
			64 → 68	0.54913	n→π*
			65 → 68	0.26873	n→π*
$S_0 \rightarrow T_4$	3.8974 eV/318.12 nm	0.0000	62 → 68	0.23531	π→π*,n→π*
			62 → 70	0.10237	π→π*,n→π*
			66 → 68	0.28422	π→π*,n→π*
			66 → 69	0.17293	π→π*,n→π*
			67 → 69	0.50161	π→π*,n→π*
			67 → 70	0.12086	π→π*,n→π*
$S_0 \rightarrow T_5$	3.9636 eV/312.81 nm	0.0000	62 → 68	0.48205	π→π*,n→π*
			62 → 70	0.10435	π→π*,n→π*
			63 → 68	0.17881	π→π*,n→π*
			66 → 70	0.13349	π→π*,n→π*
			67 → 69	0.29784	π→π*,n→π*
			67 → 70	0.26983	π→π*,n→π*

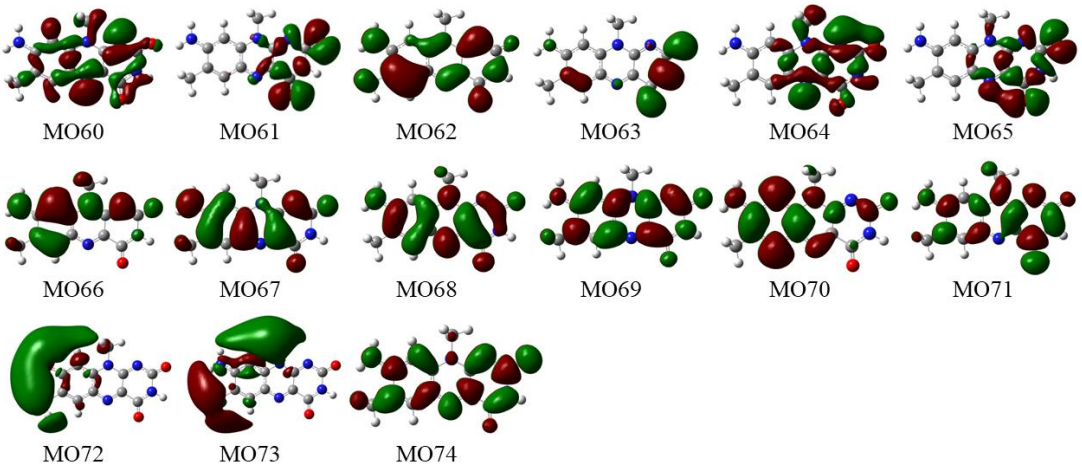

Figure S7. Isosurface plots of frontier molecular orbitals of 8Am7MeFL involved in electron transitions contribute to UV-vis absorption. (Isovalue: ±0.02 a.u.; C: Gray; O: Red; N: Blue; H: White.)

Table S8. Electronic transitions involved in the excitation of 7Am8MeFL calculated at CAM-B3LYP/6-311G(d) level of theory.

	Energy	f	Composition	CI	Character
$S_0 \rightarrow S_1$	2.9050 eV/426.80 nm	0.2778	67 → 68	0.69895	π→π*,n→π*
$S_0 \rightarrow S_2$	3.7526 eV/330.39 nm	0.0014	60 → 68	0.18628	n→π*
			63 → 68	0.50376	n→π*
			65 → 68	0.43318	n→π*
$S_0 \rightarrow S_3$	4.0391 eV/306.96 nm	0.2804	66 → 68	0.68749	π→π*,n→π*
			67 → 69	0.12427	π→π*,n→π*
$S_0 \rightarrow S_4$	4.0391 eV/306.96 nm	0.0000	61 → 68	0.28663	n→π*
			63 → 68	0.38686	n→π*
			65 → 68	0.45140	n→π*
			65 → 71	0.12996	n→π*
$S_0 \rightarrow S_5$	4.6929 eV/264.20 nm	0.1595	62 → 68	0.21543	n→π*
			64 → 68	0.45835	π→π*,n→π*
			67 → 69	0.44905	π→π*,n→π*
			67 → 70	0.10357	π→π*,n→π*
$S_0 \rightarrow S_6$	5.0509 eV/245.47 nm	0.7359	64 → 68	0.47235	π→π*,n→π*
			66 → 68	0.10188	π→π*,n→π*
			67 → 69	0.47971	π→π*,n→π*
$S_0 \rightarrow S_7$	5.1198 eV/242.17 nm	0.0027	60 → 68	0.33485	n→π*
			61 → 68	0.45288	n→π*
			63 → 68	0.21108	n→π*
			63 → 69	0.20513	n→π*
			65 → 68	0.16196	n→π*
			65 → 69	0.12019	n→π*
$S_0 \rightarrow S_8$	5.2396 eV/236.63 nm	0.0022	60 → 68	0.49403	n→π*
			61 → 68	0.31296	n→π*
			63 → 69	0.17399	n→π*
			65 → 68	0.17003	n→π*
			65 → 69	0.21627	n→π*
$S_0 \rightarrow S_9$	5.2507 eV/236.13 nm	0.1295	62 → 68	0.59858	n→π*
			66 → 69	0.13088	π→π*,n→π*
			67 → 69	0.12453	π→π*,n→π*
			67 → 70	0.27105	π→π*,n→π*
$S_0 \rightarrow S_{10}$	5.3186 eV/233.11 nm	0.1069	62 → 68	0.26120	n→π*
			64 → 68	0.17903	π→π*,n→π*
			66 → 69	0.16686	π→π*,n→π*
			67 → 70	0.57875	π→π*,n→π*
$S_0 \rightarrow T_1$	1.8853 eV/657.63 nm	0.0000	66 → 68	0.14033	π→π*,n→π*
			67 → 68	0.68334	π→π*,n→π*
			68 → 67	0.10402	π*→π,π*→n
$S_0 \rightarrow T_2$	1.8853 eV/657.63 nm	0.0000	58 → 68	0.11472	π→π*,n→π*
			64 → 68	0.12589	π→π*,n→π*

			66 → 68	0.58757	π→π*,n→π*
			66 → 70	0.16030	π→π*,n→π*
			67 → 68	0.10852	π→π*,n→π*
			67 → 69	0.20645	π→π*,n→π*
			67 → 70	0.14078	π→π*,n→π*
$S_0 \rightarrow T_3$	1.8853 eV/657.63 nm	0.0000	60 → 68	0.28120	n→π*
			63 → 68	0.48021	n→π*
			65 → 68	0.38413	n→π*
$S_0 \rightarrow T_4$	1.8853 eV/657.63 nm	0.0000	64 → 68	0.33331	π→π*,n→π*
			66 → 68	0.24611	π→π*,n→π*
			67 → 69	0.51119	π→π*,n→π*
			67 → 70	0.12543	π→π*,n→π*
$S_0 \rightarrow T_5$	1.8853 eV/657.63 nm	0.0000	64 → 68	0.37677	π→π*,n→π*
			66 → 68	0.13888	π→π*,n→π*
			67 → 69	0.27358	π→π*,n→π*
			67 → 70	0.41591	π→π*,n→π*
			67 → 71	0.17185	π→π*,n→π*
			67 → 74	0.10022	π→π*,n→π*

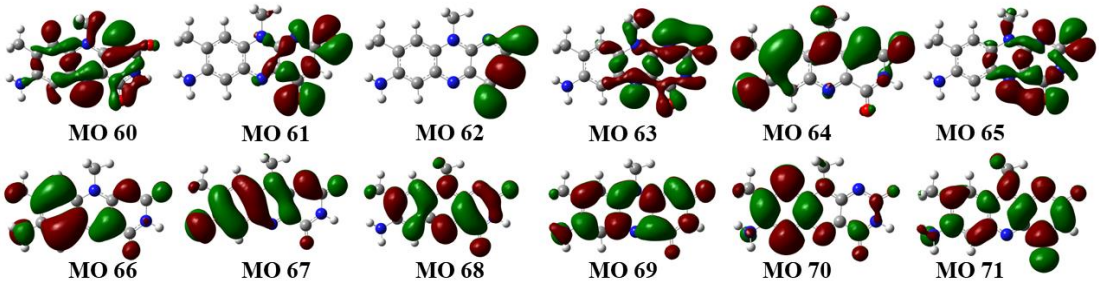

Figure S8. Isosurface plots of frontier molecular orbitals of 7Am8MeFL involved in electron transitions contribute to UV-vis absorption. (Isovalue: ±0.02 a.u.; C: Gray; O: Red; N: Blue; H: White.)

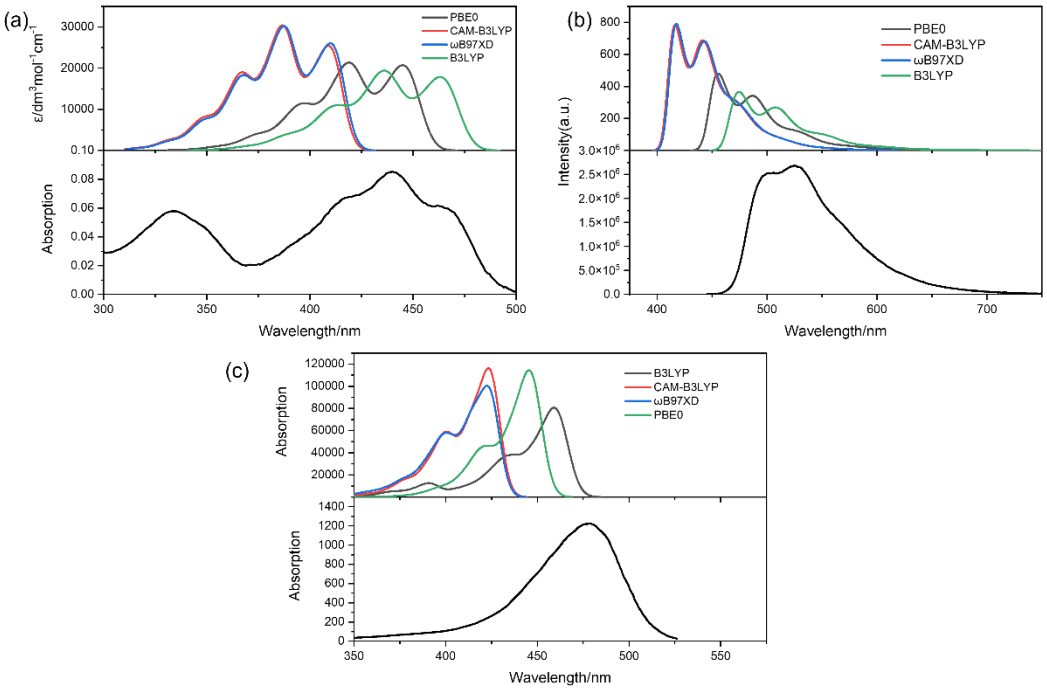

Figure S9. Comparison of calculated and experimental absorption spectra of FL(a), calculated and experimental fluorescent spectra of FL(b) and calculated and experimental spectra of 8Am7MeFL(c).

Table S9. Fluorescent properties of AmFLs investigated at TD-DFT/CAM-B3LYP /6-311g(d) level of theory

AmFL	Energy	f	Composition	CI	Character
FL	2.85 eV/435 nm	0.3911	MO 59 →MO 60	0.70193	π→π*,n→π*
9AmFL	2.09 eV/593 nm	0.0401	MO 63 →MO 64	0.70520	π→π*,n→π*
8AmFL	2.91 eV/425 nm	0.8829	MO 63 →MO 64	0.69777	π→π*,n→π*
7AmFL	2.20 eV/564 nm	0.2428	MO 63 →MO 64	0.70366	π→π*,n→π*
6AmFL	2.39 eV/518 nm	0.1785	MO 63 →MO 64	0.70411	π→π*,n→π*
8Am7MeFL	2.88 eV/430 nm	0.8879	MO 67 →MO 68	0.69808	π→π*,n→π*

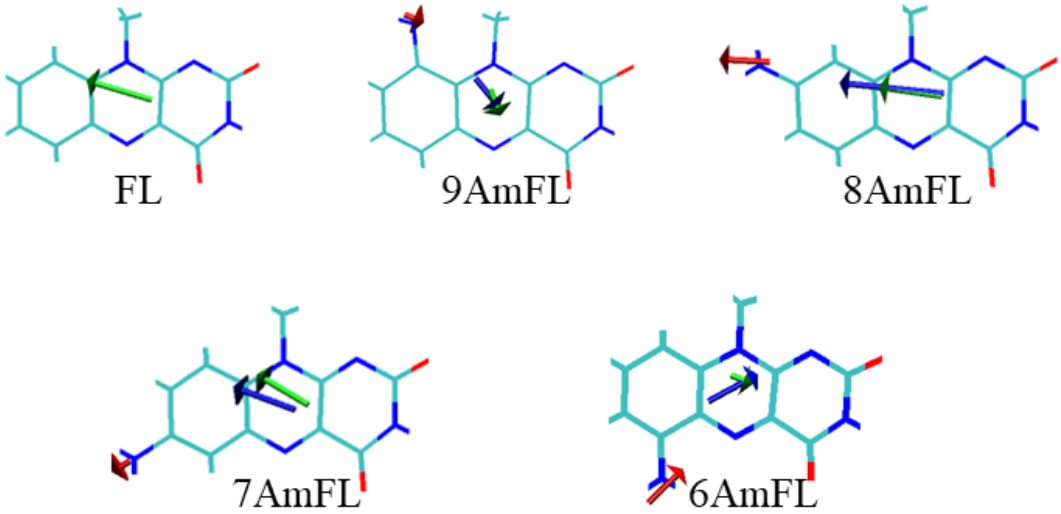

Figure S10. Contribution of $-NH_2$ (red) and isoalloxazine moiety (green) to $\mu(S_0 \rightarrow S_1)$ of FL, 9AmFL, 8AmFL, 7AmFL and 6AmFL (blue).

Table S10. Contribution of $-NH_2$ and isoalloxazine moiety to $\mu(S_0 \rightarrow S_1)$ of FL, 9AmFL, 8AmFL, 7AmFL and 6AmFL.

Mol	$\lvert\mu(S_0 \rightarrow S_1)\rvert^a$ (a.u.)	Contribution of isoalloxazine to $\lvert\mu(S_0 \rightarrow S_1)\rvert$ (a.u.)	Contribution of $-NH_2$ to $\lvert\mu(S_0 \rightarrow S_1)\rvert$ (a.u.)
FL	2.01	——	——
9AmFL	0.93	0.62	0.40
8AmFL	3.01	1.72	1.30
7AmFL	1.79	1.59	0.36
6AmFL	1.51	0.46	1.26

[a] The transition dipole moments were calculated as vectors, they were projected to calculate the contribution of $-NH_2$ and isoalloxazine moieties. For clearance, only $|\mu|$ was presented.

Table S11. Hole-electron analysis of excited states of AmFLs performed at CAM-B3LYP/6-311g(d) level of theory with Multiwfn.

AmFL	D/Å[a]	S_r/a.u.[b]	H/Å[c]	t/Å[d]	HDI[e]	EDI[f]
FL: S_1	0.86	0.71	2.67	-0.40	9.04	9.14
FL:S_2	2.27	0.42	2.24	0.70	22.62	10.08
FL: T_1	0.47	0.78	2.61	-0.86	8.60	9.27
FL: T_2	0.81	0.88	2.57	-1.17	7.89	7.49
FL: T_3	0.36	0.57	2.07	-0.98	17.50	11.44
9AmFL: S_1	1.88	0.64	2.58	0.01	8.60	9.19
9AmFL: T_1	1.16	0.72	2.64	-0.63	8.55	8.60
9AmFL: T_2	0.63	0.83	2.66	-1.54	7.65	8.28
8AmFL: S_1	0.67	0.75	2.88	-1.56	8.13	9.15
8AmFL:S_2	1.95	0.61	2.52	0.11	9.84	9.57
8AmFL: T_1	0.50	0.75	2.82	-1.61	8.18	9.39
8AmFL: T_2	0.91	0.79	2.76	-0.77	8.95	7.72
8AmFL: T_3	0.49	0.57	2.11	-0.90	18.00	11.58
7AmFL: S_1	1.37	0.70	2.84	-0.97	8.17	8.87
7AmFL: T_1	0.75	0.75	2.82	-1.39	7.78	8.69
6AmFL: S_1	2.10	0.57	2.41	0.45	9.90	9.26
6AmFL: T_1	0.71	0.75	2.56	-1.29	8.47	9.23
6AmFL: T_2	0.79	0.71	2.75	-0.78	8.64	8.61
8Am7MeFL: S_1	0.61	0.75	2.90	-1.48	8.01	9.12
8Am7MeFL: T_1	0.48	0.75	2.84	-1.52	8.05	9.34
8Am7MeFL: T_2	0.90	0.80	2.78	-0.83	8.59	7.67
7Am8MeFL: S_1	1.29	0.71	2.87	-1.11	8.00	8.96
7Am8MeFL: T_1	0.73	0.76	2.85	-1.55	7.64	8.78

[a.] The distance between centroids of hole and electron. [b.] The overlap between hole and electron, calculated as $\int \sqrt{\rho^{hole}(\mathbf{r})\rho^{ele}(\mathbf{r})}\, d\mathbf{r}$, where $\rho^{hole}(\mathbf{r})$ and $\rho^{ele}(\mathbf{r})$ are the density distribution of hole and electron, respectively. [c.] Averaged root mean square derivation of spatial extension of hole and electron distribution, calculated as $H = (|\sigma_{ele}| + |\sigma_{hole}|)/2$, where $|\sigma_{ele}|$ and $|\sigma_{hole}|$ measure the overall root mean square derivation of electron and hole, respectively. [d.] The degree of separation of hole and electron in the direction of charge transfer, calculated as $t = D - H_{CT}$, where D is the distance between centroids of hole and electron, and H_{CT} is the averaged degree of spatial extension of hole and electron distribution in CT direction. [e.] The hole delocalization index, calculated as $100 \times \sqrt{\int [\rho^{hole}(\mathbf{r})]^2 d\mathbf{r}}$. [f.] The electron delocalization index, calculated as $100 \times \sqrt{\int [\rho^{ele}(\mathbf{r})]^2 d\mathbf{r}}$.

Table S12. Isosurface plots of charge density difference (CDD) and hole-electron (h-e) plots of excited states of AmFLs performed at CAM-B3LYP/6-311g(d) level of theory (Isovalue: ±0.002 a.u.).

States		FL	9AmFL	8AmFL	7AmFL	6AmFL	7Am8MeFL	8Am7MeFL
S_1	CDD	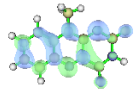	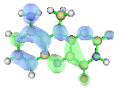	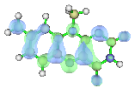	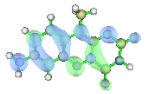	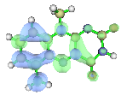	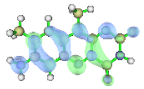	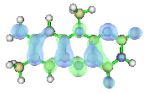
	h-e	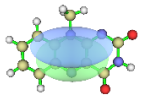	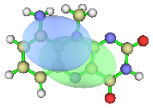	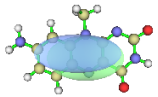	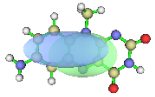	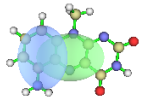	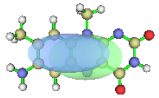	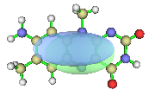
S_2	CDD	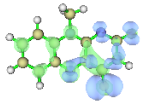		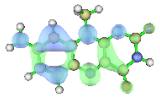				
	h-e	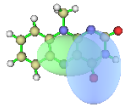		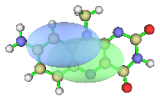				
T_1	CDD	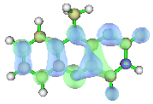	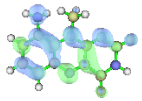	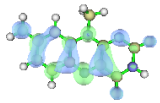	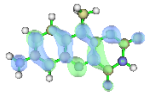	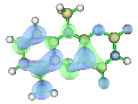	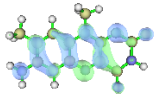	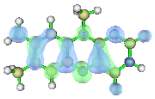
	h-e	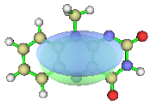	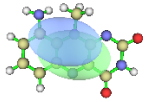	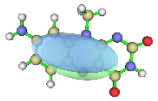	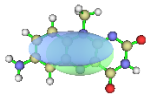	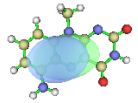	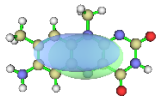	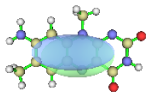
T_2	CDD	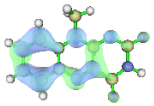	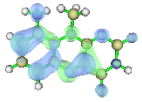	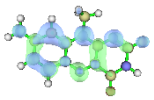		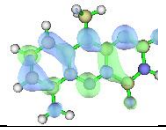		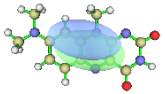

	h-e	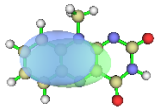	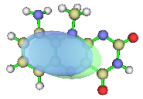	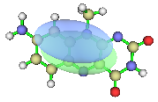	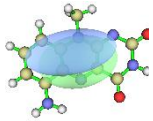	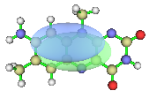
T_3	CDD	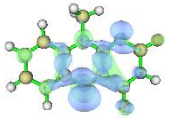		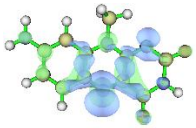		
	h-e	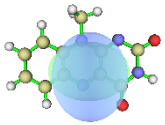		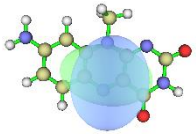		

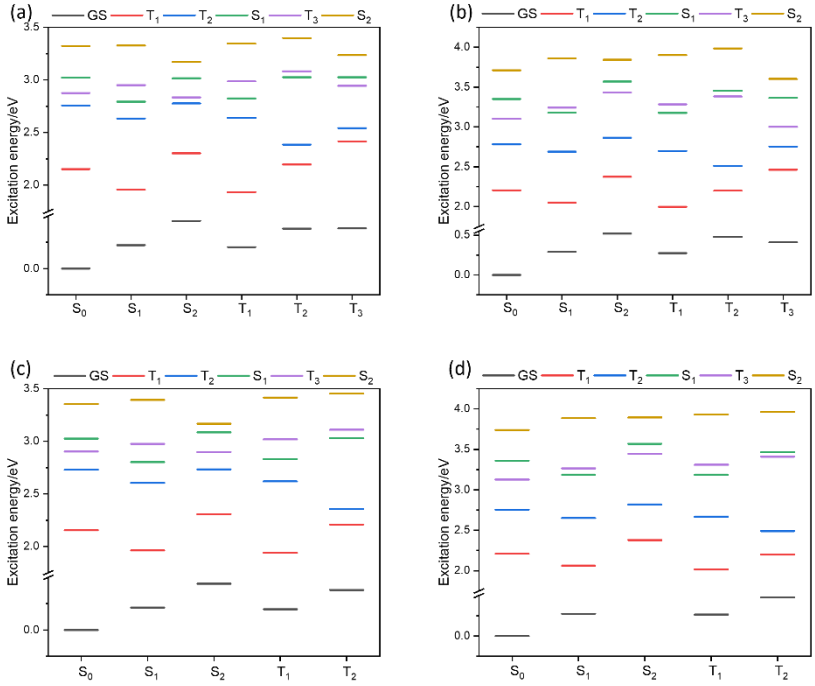

Figure S11. Vertical excitation energy of FL in DCM (a,b) and water(c,d) calculated with B3LYP(a,c) and CAM-B3LYP (b,d) functional at S_0, S_1, S_2, T_1, T_2 and T_3 minimum geometry obtained at B3LYP/6-311g(d) level of theory.

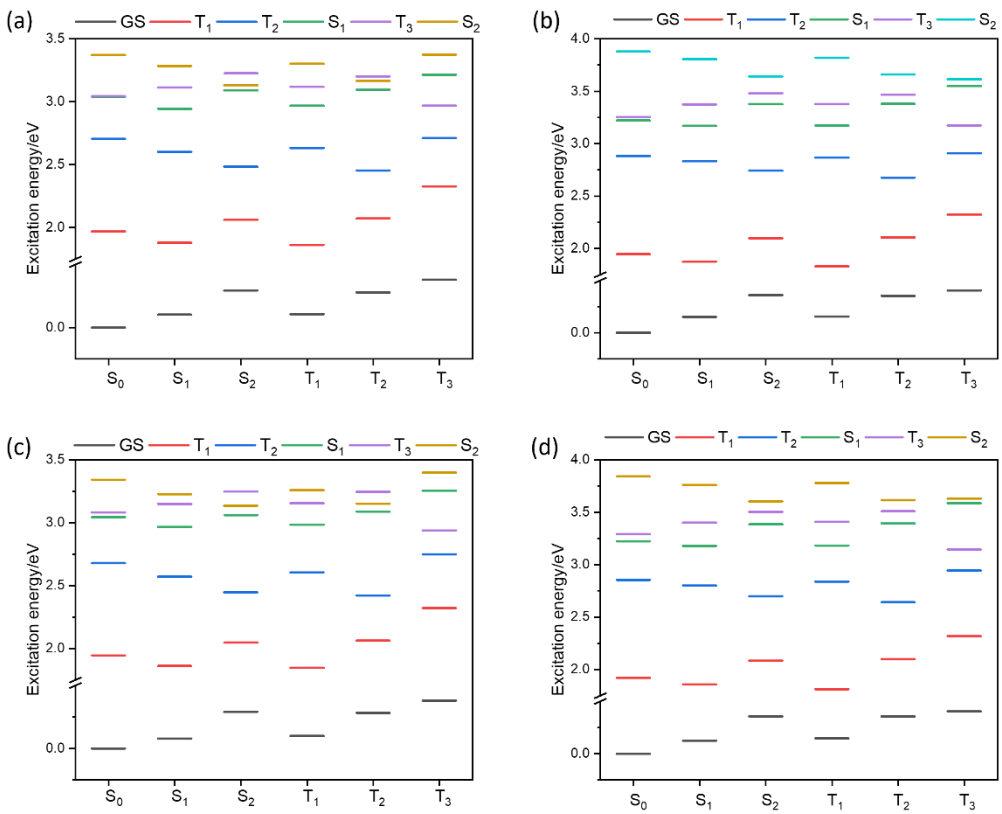

Figure S12. Vertical excitation energy of 8AmFL in DCM (a,b) and water(c,d) calculated with B3LYP(a,c) and CAM-B3LYP (b,d) functional at S_0, S_1, S_2, T_1, T_2 and T_3 minimum geometry obtained at B3LYP/6-311g(d) level of theory.

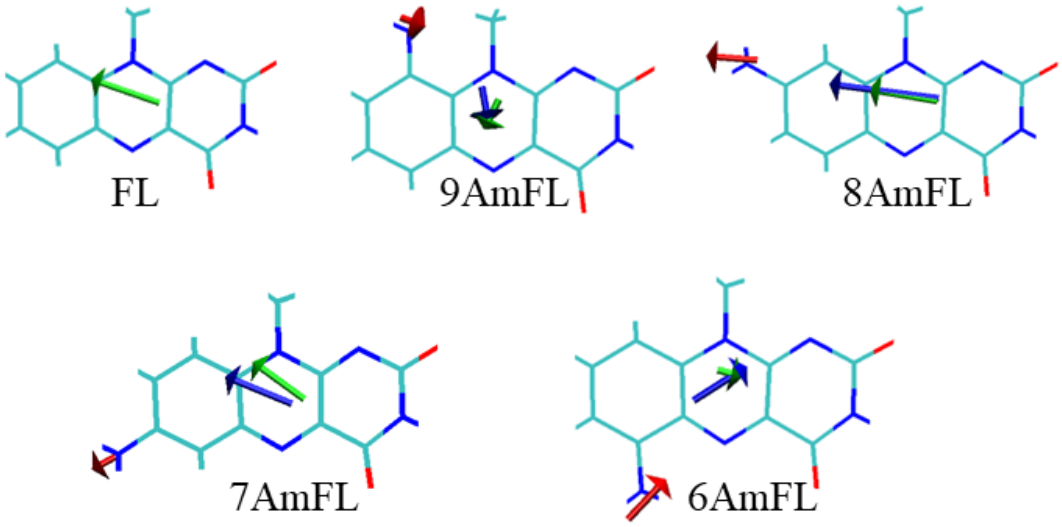

Figure S13. Contribution of $-NH_2$ (red) and isoalloxazine moiety (green) to $\mu(S_1 \rightarrow S_0)$ of FL, 9AmFL, 8AmFL, 7AmFL and 6AmFL (blue).

Table S13. Contribution of $-NH_2$ and isoalloxazine moiety to $\mu(S_1 \rightarrow S_0)$ of FL, 9AmFL, 8AmFL, 7AmFL and 6AmFL.

Mol	$\lvert\mu(S_1 \rightarrow S_0)\rvert^a$ (a.u.)	Contribution of isoalloxazine to $\lvert\mu(S_1 \rightarrow S_0)\rvert$ (a.u.)	Contribution of $-NH_2$ to $\lvert\mu(S_1 \rightarrow S_0)\rvert$ (a.u.)
FL	1.63	1.63	——
9AmFL	0.56	0.45	0.73
8AmFL	2.72	1.95	0.78
7AmFL	1.48	1.29	0.33
6AmFL	0.90	0.30	0.62

[a] The transition dipole moments were calculated as vectors, they were projected to calculate the contribution of $-NH_2$ and isoalloxazine moieties. For clearance, only $|\mu|$ was presented.

Table S14. Projection of HR and E_{reorg} of $S_1 \rightarrow S_0$ transition to S_0 vibrational normal modes of FL.

S_0 Normal Mode	Frequency /cm^{-1}	HR factor	HR %	E_{reorg} / cm^{-1}	E_{reorg} %
7	210.42	0.70	30.35	147.55	7.40
13	435.64	0.04	1.84	18.53	0.93
15	516.76	0.11	4.96	59.21	2.97
17	548.24	0.12	5.15	65.17	3.27
20	625.54	0.11	4.76	68.77	3.45
21	659.41	0.02	1.03	15.65	0.79
23	729.52	0.03	1.12	18.84	0.95
28	808.55	0.07	2.84	53.08	2.66
38	1128.46	0.04	1.78	46.42	2.33
39	1155.36	0.04	1.78	47.45	2.38
41	1201.15	0.03	1.16	32.28	1.62
42	1223.66	0.03	1.35	38.07	1.91
43	1250.85	0.21	8.95	258.68	12.98
46	1357.22	0.02	0.70	22.07	1.11
47	1395.03	0.07	3.05	98.19	4.93
48	1407.42	0.12	5.40	175.46	8.80
49	1436.02	0.05	2.12	70.49	3.54
51	1470.92	0.02	0.89	30.15	1.51
54	1528.74	0.02	1.02	36.00	1.81
57	1633.95	0.14	6.22	234.74	11.78
58	1673.12	0.09	4.08	157.76	7.92
59	1701.61	0.11	4.89	192.18	9.64
60	1786.49	0.02	0.83	34.40	1.73

Note: Total E_{reorg} is 1993 cm^{-1} and total HR is 2.31.

Table S15. Projection of HR and E_{reorg} of $S_1 \rightarrow S_0$ transition to S_0 vibrational normal modes of 6AmFL.

S_0 Normal Mode	Frequency /cm^{-1}	HR factor	HR %	E_{reorg} / cm^{-1}	E_{reorg} %
7	182.35	0.15	5.75	27.64	1.28
10	303.60	0.10	3.75	29.95	1.39
12	344.30	0.08	2.90	26.30	1.22
15	426.68	0.26	9.97	112.09	5.21
16	440.22	0.04	1.43	16.63	0.77
20	545.86	0.49	18.55	266.66	12.39
21	550.15	0.47	17.88	259.04	12.04
24	642.89	0.12	4.50	76.13	3.54
27	728.95	0.03	1.25	23.91	1.11
30	780.87	0.04	1.46	30.02	1.40
41	1092.33	0.06	2.13	61.38	2.85
45	1220.55	0.08	2.94	94.53	4.39
46	1233.83	0.02	0.69	22.53	1.05
48	1316.77	0.05	1.75	60.68	2.82
49	1348.82	0.03	1.17	41.53	1.93
50	1380.90	0.02	0.65	23.51	1.09
59	1555.87	0.02	0.92	37.74	1.75
60	1586.77	0.04	1.67	69.90	3.25
61	1626.88	0.13	5.08	217.69	10.12
63	1669.04	0.10	3.74	164.55	7.65
64	1688.46	0.22	8.39	373.23	17.35

Note: Total E_{reorg} is 2152 cm^{-1} and total HR is 2.63.

Table S16. Projection of HR and E_{reorg} of $S_1 \rightarrow S_0$ transition to S_0 vibrational normal modes of 7AmFL.

S_0 Normal Mode	Frequency /cm^{-1}	HR factor	HR %	E_{reorg} / cm^{-1}	E_{reorg} %
6	179.22	0.47	11.04	84.79	2.33
10	300.03	0.18	4.16	53.46	1.47
13	355.88	0.12	2.89	44.09	1.21
15	415.04	0.11	2.59	46.03	1.26
18	509.58	0.31	7.16	156.35	4.30
20	526.46	0.56	13.12	295.93	8.13
21	536.59	0.88	20.51	471.72	12.96
23	623.89	0.12	2.85	76.19	2.09
25	660.86	0.06	1.42	40.27	1.11
31	804.35	0.06	1.41	48.57	1.33
42	1135.25	0.05	1.14	55.53	1.53
44	1196.39	0.03	0.79	40.45	1.11
45	1210.34	0.05	1.14	59.18	1.63
46	1240.02	0.04	1.01	53.77	1.48
47	1281.52	0.08	1.91	104.66	2.88
50	1366.53	0.06	1.38	80.75	2.22
51	1398.59	0.14	3.21	192.22	5.28
58	1532.08	0.03	0.75	48.95	1.34
60	1592.34	0.04	0.91	62.41	1.71
61	1631.64	0.02	0.54	37.51	1.03
62	1681.75	0.15	3.40	245.11	6.73
63	1698.01	0.14	3.19	232.45	6.39

Note: Total E_{reorg} is 3640 cm^{-1} and total HR is 4.29.

Table S17. Projection of HR and E_{reorg} of $S_1 \rightarrow S_0$ transition to S_0 vibrational normal modes of 8AmFL.

S_0 Normal Mode	Frequency /cm^{-1}	HR factor	HR %	E_{reorg} / cm^{-1}	E_{reorg} %
7	185.55	0.08	8.01	14.96	1.67
14	388.10	0.05	4.91	19.18	2.15
19	509.51	0.06	6.26	32.07	3.59
21	534.59	0.20	19.58	105.33	11.78
23	608.52	0.06	5.97	36.53	4.09
25	667.93	0.01	1.02	6.85	0.77
30	793.53	0.02	2.10	16.75	1.87
34	857.46	0.07	6.82	58.84	6.58
37	969.21	0.01	0.98	9.57	1.07
42	1120.68	0.03	2.74	30.93	3.46
45	1234.80	0.01	0.82	10.23	1.14
46	1241.72	0.02	2.00	24.99	2.80
47	1300.22	0.03	3.01	39.37	4.40
49	1341.26	0.01	1.44	19.48	2.18
50	1379.24	0.02	2.08	28.88	3.23
51	1403.35	0.08	7.86	111.00	12.42
55	1488.54	0.01	0.69	10.34	1.16
59	1571.06	0.02	2.19	34.57	3.87
60	1589.86	0.07	6.55	104.82	11.73
62	1626.58	0.05	4.57	74.81	8.37
64	1710.35	0.02	2.15	36.92	4.13

Note: Total E_{reorg} is 893 cm^{-1} and total HR is 1.01.

Table S18. Projection of HR and E_{reorg} of $S_1 \rightarrow S_0$ transition to S_0 vibrational normal modes of 9AmFL.

S_0 Normal Mode	Frequency /cm^{-1}	HR factor	HR %	E_{reorg} / cm^{-1}	E_{reorg} %
2	70.13	2.49	28.10	174.81	3.70
3	119.04	0.56	6.26	66.10	1.40
6	185.64	0.33	3.74	61.62	1.30
7	201.57	0.35	3.98	71.11	1.50
9	282.89	0.09	1.06	26.48	0.56
10	304.76	0.09	1.04	28.03	0.59
13	378.36	0.24	2.67	89.68	1.90
14	394.81	0.19	2.11	73.93	1.56
18	511.04	0.16	1.81	82.04	1.73
21	566.72	0.22	2.52	126.55	2.68
22	597.79	0.14	1.61	85.33	1.80
23	609.30	0.40	4.46	241.20	5.10
24	629.63	0.23	2.58	144.12	3.05
25	671.90	0.08	0.88	52.38	1.11
26	712.50	1.09	12.30	777.70	16.44
28	741.24	0.17	1.92	126.29	2.67
29	754.42	0.25	2.82	188.46	3.98
30	767.91	0.12	1.32	90.14	1.91
35	879.93	0.05	0.62	48.38	1.02
42	1132.64	0.06	0.70	70.02	1.48
45	1207.55	0.04	0.47	50.22	1.06
46	1247.07	0.13	1.45	160.97	3.40
50	1351.72	0.09	0.98	117.13	2.48
51	1387.38	0.16	1.81	222.78	4.71
52	1411.16	0.09	0.98	123.25	2.61
59	1548.92	0.06	0.67	92.14	1.95
62	1670.63	0.21	2.35	347.65	7.35
63	1696.17	0.38	4.23	637.07	13.47

Note: Total E_{reorg} is 4730 cm^{-1} and total HR is 8.87.

Table S19. Calculated rate constants for IC among energy allowed transitions among T_n of AmFLs (s^{-1}).

298 K	$T_3 \rightarrow T_2$ k_{IC}[a]	$T_2 \rightarrow T_1$ k_{IC}[b]	$T_3 \rightarrow T_1$ k_{IC}[c]
FL	3.69×10^{12}	7.68×10^{12}	8.10×10^{11}
6AmFL	——	4.94×10^{12}	——
7AmFL	——	4.08×10^{12}	——
8AmFL	6.46×10^{11}	4.63×10^{12}	1.62×10^{12}
9AmFL	——	2.64×10^{12}	——

[a] Rate constants for $T_3 \rightarrow T_2$ IC; [b] Rate constants for $T_2 \rightarrow T_1$ IC; [c] Rate constants for $T_3 \rightarrow T_1$ IC.

Table S20. Calculated rate constants for radiative and nonradiative $T_n \rightarrow S_0$ transitions of AmFL derivatives（s^{-1}）

298 K	T_1-S_0 k'_{ISC}[a]	T_1-S_0 k_p[b]	T_2-S_0 k'_{ISC}[c]	T_2-S_0 k_p[d]	T_3-S_0 k'_{ISC}[e]	T_3-S_0 k_p[f]
FL	1.60×10^{6}	1.30×10^{-2}	4.16×10^{4}	8.44×10^{-2}	3.23×10^{4}	4.29×10^{-1}
6AmFL	6.66×10^{2}	8.35×10^{-3}	1.01×10^{5}	3.62×10^{-2}	——	——
7AmFL	7.17×10^{4}	5.10×10^{-3}	2.12×10^{5}	1.62×10^{-2}	——	——
8AmFL	7.43×10^{2}	3.71×10^{-2}	4.03×10^{6}	6.42×10^{-2}	6.94×10^{6}	1.10×10^{-1}
9AmFL	6.69×10^{5}	4.91×10^{-3}	1.14×10^{6}	2.18×10^{-2}	——	——

[a] Nonradiative decay rate constants for the $T_1 \rightarrow S_0$ transition; [b] Radiative decay rate constants for the $T_1 \rightarrow S_0$ transition; [c] Nonradiative decay rate constants for the $T_2 \rightarrow S_0$ transition; [d] Radiative decay rate constants for the $T_2 \rightarrow S_0$ transition; [e] Nonradiative decay rate constants for the $T_3 \rightarrow S_0$ transition; [f] Radiative decay rate constants for the $T_3 \rightarrow S_0$ transition.

Table S21. Projection of HR and E_{reorg} of $T_1 \rightarrow S_0$ transition to S_0 vibrational normal modes of FL.

S_0 Normal Mode	Frequency /cm^{-1}	HR factor	HR %	E_{reorg} / cm^{-1}	E_{reorg} %
2	86.07	0.14	4.05	12.23	0.30
12	391.10	0.16	4.65	63.91	1.54
13	435.64	0.05	1.36	20.76	0.50
15	516.76	0.62	17.62	319.73	7.72
28	808.55	0.16	4.49	127.35	3.08
30	864.69	0.07	2.10	63.66	1.54
39	1155.36	0.06	1.59	64.68	1.56
43	1250.85	0.10	2.97	130.34	3.15
44	1320.34	0.05	1.53	70.89	1.71
47	1395.03	0.06	1.82	88.99	2.15
48	1407.42	0.06	1.71	84.58	2.04
49	1436.02	0.04	1.03	51.78	1.25
52	1507.97	0.03	0.82	43.56	1.05
54	1528.74	0.06	1.70	91.49	2.21
56	1600.14	0.22	6.31	354.34	8.56
57	1633.95	0.72	20.56	1179.44	28.48
58	1673.12	0.64	18.21	1069.74	25.83
60	1786.49	0.05	1.43	89.51	2.16

Note: Total E_{reorg} is 4141 cm^{-1} and total HR is 3.51.

Table S22. Projection of HR and E_{reorg} of $T_1 \rightarrow S_0$ transition to S_0 vibrational normal modes of 6AmFL.

S_0 Normal Mode	Frequency /cm^{-1}	HR factor	HR %	E_{reorg} / cm^{-1}	E_{reorg} %
7	182.35	0.10	3.25	18.81	0.64
14	362.09	0.06	1.97	22.60	0.77
15	426.68	0.26	8.25	111.79	3.79
18	521.93	0.05	1.69	28.02	0.95
20	545.86	0.36	11.30	195.84	6.64
21	550.15	0.82	25.90	452.42	15.34
30	780.87	0.08	2.54	63.07	2.14
34	861.52	0.04	1.18	32.37	1.10
44	1198.61	0.06	1.74	66.16	2.24
46	1233.83	0.06	1.83	71.53	2.42
48	1316.77	0.16	4.93	206.26	6.99
50	1380.90	0.03	1.09	47.88	1.62
51	1389.00	0.06	1.91	84.12	2.85
56	1505.25	0.04	1.22	58.33	1.98
59	1555.87	0.03	1.00	49.17	1.67
60	1586.77	0.26	8.34	420.05	14.24
61	1626.88	0.46	14.60	754.13	25.56
63	1669.04	0.06	1.86	98.58	3.34

Note: Total E_{reorg} is 2950 cm^{-1} and total HR is 3.18

Table S23. Projection of HR and E_{reorg} of $T_1 \rightarrow S_0$ transition to S_0 vibrational normal modes of 7AmFL.

S_0 Normal Mode	Frequency /cm^{-1}	HR factor	HR %	E_{reorg} / cm^{-1}	E_{reorg} %
6	179.22	0.58	12.04	104.73	2.50
10	300.03	0.16	3.30	48.08	1.15
13	355.88	0.14	2.95	50.98	1.22
15	415.04	0.09	1.95	39.34	0.94
18	509.58	0.35	7.26	179.56	4.29
20	526.46	0.64	13.13	335.53	8.02
21	536.59	0.85	17.45	454.32	10.86
23	623.89	0.17	3.58	108.52	2.59
31	804.35	0.09	1.93	75.31	1.80
41	1122.51	0.04	0.81	44.26	1.06
42	1135.25	0.07	1.45	79.90	1.91
45	1210.34	0.06	1.33	78.01	1.87
47	1281.52	0.09	1.89	117.84	2.82
50	1366.53	0.10	2.12	140.61	3.36
51	1398.59	0.27	5.59	379.10	9.06
53	1437.88	0.03	0.66	46.19	1.10
58	1532.08	0.05	1.11	82.33	1.97
60	1592.34	0.07	1.48	114.15	2.73
61	1631.64	0.03	0.53	42.14	1.01
62	1681.75	0.13	2.64	215.61	5.16
63	1698.01	0.18	3.66	301.50	7.21
73	3607.74	0.21	4.33	758.25	18.13
75	3701.89	0.01	0.31	55.51	1.33

Note: Total E_{reorg} is 4182 cm^{-1} and total HR is 4.85.

Table S24. Projection of HR and E_{reorg} of $T_1 \rightarrow S_0$ transition to S_0 vibrational normal modes of 8AmFL.

S_0 Normal Mode	Frequency /cm^{-1}	HR factor	HR %	E_{reorg} / cm^{-1}	E_{reorg} %
7	185.55	0.08	4.85	15.63	0.93
14	388.10	0.15	8.73	58.87	3.51
16	440.93	0.02	1.19	9.08	0.54
19	509.51	0.08	4.80	42.51	2.53
21	534.59	0.30	17.50	162.55	9.68
22	563.00	0.04	2.02	19.79	1.18
23	608.52	0.04	2.56	27.05	1.61
30	793.53	0.03	1.97	27.11	1.61
34	857.46	0.13	7.75	115.38	6.87
42	1120.68	0.02	1.06	20.56	1.22
46	1241.72	0.04	2.04	43.94	2.62
47	1300.22	0.03	1.70	38.40	2.29
49	1341.26	0.02	0.89	20.71	1.23
51	1403.35	0.11	6.30	153.66	9.15
56	1510.19	0.02	1.15	30.09	1.79
57	1524.24	0.09	4.97	131.71	7.84
59	1571.06	0.05	3.00	81.97	4.88
60	1589.86	0.20	11.55	318.88	18.99
61	1602.26	0.07	3.80	105.74	6.30
62	1626.58	0.08	4.66	131.74	7.85
65	1774.78	0.01	0.64	19.80	1.18

Note: Total E_{reorg} is 1679 cm^{-1} and total HR is 1.74.

Table S25. Projection of HR and E_{reorg} of $T_1 \rightarrow S_0$ transition to S_0 vibrational normal modes of 9AmFL.

S_0 Normal Mode	Frequency /cm^{-1}	HR factor	HR %	E_{reorg} / cm^{-1}	E_{reorg} %
2	70.13	1.30	15.64	91.13	1.67
3	119.04	0.33	3.94	38.98	0.71
6	185.64	0.40	4.78	73.65	1.35
7	201.57	0.30	3.65	61.11	1.12
10	304.76	0.19	2.27	57.35	1.05
13	378.36	0.36	4.33	135.99	2.49
14	394.81	0.23	2.78	91.34	1.67
18	511.04	0.17	2.06	87.28	1.60
19	532.60	0.09	1.12	49.38	0.90
21	566.72	0.18	2.14	100.83	1.85
22	597.79	0.09	1.07	52.97	0.97
23	609.30	0.39	4.68	236.73	4.34
24	629.63	0.15	1.86	97.52	1.79
25	671.90	0.10	1.15	64.22	1.18
26	712.50	1.14	13.70	810.84	14.86
28	741.24	0.18	2.15	132.38	2.43
29	754.42	0.31	3.73	233.83	4.28
30	767.91	0.12	1.41	90.19	1.65
35	879.93	0.09	1.05	76.85	1.41
41	1108.69	0.06	0.68	62.98	1.15
42	1132.64	0.11	1.30	122.73	2.25
46	1247.07	0.15	1.81	187.83	3.44
50	1351.72	0.13	1.61	180.79	3.31
51	1387.38	0.30	3.61	416.41	7.63
52	1411.16	0.11	1.33	155.80	2.85
59	1548.92	0.07	0.80	102.53	1.88
62	1670.63	0.36	4.31	598.27	10.96
63	1696.17	0.33	4.00	563.45	10.32

Note: Total E_{reorg} is 5458 cm^{-1} and total HR is 8.31.

Table S26. Concentration of AmFLs at steady state under irradiation (mol/L)

Mol（298 K）	$c(S_0)$	$c(S_1)$	$c(T_1)$	$c(T_2)$	$c(T_3)$
FL	3.29×10^{-2}	4.43×10^{-8}	7.65×10^{-5}	1.31×10^{-11}	2.71×10^{-11}
8AmFL	3.01×10^{-3}	8.40×10^{-8}	3.00×10^{-2}	2.50×10^{-12}	1.64×10^{-11}

References:

1. R. C. Binning and L. A. Curtiss, *J. Comput. Chem.*, 1990, **11**, 1206-1216.
2. M. M. Francl, W. J. Pietro, W. J. Hehre, J. S. Binkley, M. S. Gordon, D. J. Defrees and J. A. Pople, *J. Chem. Phys.*, 1982, **77**, 3654-3665.
3. A. D. Becke, *J. Chem. Phys.*, 1993, **98**, 5648-5652.
4. C. T. Lee, W. T. Yang and R. G. Parr, *Phys. Rev. B*, 1988, **37**, 785-789.
5. S. Miertus, E. Scrocco and J. Tomasi, *Chem. Phys.*, 1981, **55**, 117-129.
6. R. Cammi and B. Mennucci, *J. Chem. Phys.*, 1999, **110**, 9877-9886.
7. J. Tomasi, B. Mennucci and R. Cammi, *Chem. Rev.*, 2005, **105**, 2999-3093.
8. M. J. Frisch, G. W. Trucks, H. B. Schlegel, G. E. Scuseria, M. A. Robb, J. R. Cheeseman, G. Scalmani, V. Barone, G. A. Petersson, H. Nakatsuji, X. Li, M. Caricato, A. V. Marenich, J. Bloino, B. G. Janesko, R. Gomperts, B. Mennucci, H. P. Hratchian, J. V. Ortiz, A. F. Izmaylov, J. L. Sonnenberg, Williams, F. Ding, F. Lipparini, F. Egidi, J. Goings, B. Peng, A. Petrone, T. Henderson, D. Ranasinghe, V. G. Zakrzewski, J. Gao, N. Rega, G. Zheng, W. Liang, M. Hada, M. Ehara, K. Toyota, R. Fukuda, J. Hasegawa, M. Ishida, T. Nakajima, Y. Honda, O. Kitao, H. Nakai, T. Vreven, K. Throssell, J. A. Montgomery Jr., J. E. Peralta, F. Ogliaro, M. J. Bearpark, J. J. Heyd, E. N. Brothers, K. N. Kudin, V. N. Staroverov, T. A. Keith, R. Kobayashi, J. Normand, K. Raghavachari, A. P. Rendell, J. C. Burant, S. S. Iyengar, J. Tomasi, M. Cossi, J. M. Millam, M. Klene, C. Adamo, R. Cammi, J. W. Ochterski, R. L. Martin, K. Morokuma, O. Farkas, J. B. Foresman and D. J. Fox, *Journal*, 2016.
9. J. Wang and B. Durbeej, *J. Comput. Chem.*, 2020, **41**, 1718-1729.
10. Y.-K. Choe, S. Nagase and K. Nishimoto, *J. Comput. Chem.*, 2007, **28**, 727-739.
11. R. K. Kar, S. Chasen, M. A. Mroginski and A. F. Miller, *J. Phys. Chem. B*, 2021, **125**, 12654-12669.
12. B. D. Etz, J. M. DuClos and S. Vyas, *J. Phys. Chem. A*, 2020, **124**, 4193-4201.
13. O. Vahtras, H. Agren, P. Jorgensen, H. J. A. Jensen, T. Helgaker and J. Olsen, *J. Chem. Phys.*, 1992, **97**, 9178-9187.
14. H. Hettema, H. J. A. Jensen, P. Jorgensen and J. Olsen, *J. Chem. Phys.*, 1992, **97**, 1174-1190.
15. H. Agren, O. Vahtras, H. Koch, P. Jorgensen and T. Helgaker, *J. Chem. Phys.*, 1993, **98**, 6417-6423.
16. J. Olsen, D. L. Yeager and P. Jorgensen, *J. Chem. Phys.*, 1989, **91**, 381-388.
17. P. Jorgensen, H. J. A. Jensen and J. Olsen, *J. Chem. Phys.*, 1988, **89**, 3654-3661.
18. K. Aidas, C. Angeli, K. L. Bak, V. Bakken, R. Bast, L. Boman, O. Christiansen, R. Cimiraglia, S. Coriani, P. Dahle, E. K. Dalskov, U. Ekstrom, T. Enevoldsen, J. J. Eriksen, P. Ettenhuber, B. Fernandez, L. Ferrighi, H. Fliegl, L. Frediani, K. Hald, A. Halkier, C. Hattig, H. Heiberg, T. Helgaker, A. C. Hennum, H. Hettema, E. Hjertenaes, S. Host, I. M. Hoyvik, M. F. Iozzi, B. Jansik, H. J. A. Jensen, D. Jonsson, P. Jorgensen, J. Kauczor, S. Kirpekar, T. Kjrgaard, W. Klopper, S. Knecht, R. Kobayashi, H. Koch, J. Kongsted, A. Krapp, K. Kristensen, A. Ligabue, O. B. Lutnaes, J. I. Melo, K. V. Mikkelsen, R. H. Myhre, C. Neiss, C. B. Nielsen, P. Norman, J. Olsen, J. M. H. Olsen, A. Osted, M. J. Packer, F. Pawlowski, T. B. Pedersen, P. F. Provasi, S. Reine, Z. Rinkevicius, T. A. Ruden, K. Ruud, V. V. Rybkin, P. Salek, C. C. M. Samson, A. S. de Meras, T. Saue, S. P. A. Sauer, B. Schimmelpfennig, K. Sneskov, A. H. Steindal, K. O. Sylvester-Hvid, P. R. Taylor, A. M. Teale, E. I. Tellgren, D. P. Tew, A. J. Thorvaldsen, L. Thogersen, O. Vahtras, M. A. Watson, D. J. D. Wilson, M. Ziolkowski and H.

Agren, *Wiley Interdiscip. Rev.-Comput. Mol. Sci.*, 2014, **4**, 269-284.
19. Q. Peng, Y. P. Yi, Z. G. Shuai and J. S. Shao, *J. Chem. Phys.*, 2007, **126**, 114302.
20. Q. Peng, Y. P. Yi, Z. G. Shuai and J. S. Shao, *J. Am. Chem. Soc.*, 2007, **129**, 9333-9339.
21. Y. L. Niu, Q. A. Peng, C. M. Deng, X. Gao and Z. G. Shuai, *J. Phys. Chem. A*, 2010, **114**, 7817-7831.
22. Y. Niu, Q. Peng and Z. Shuai, *Sci. China Ser. B-Chem.*, 2008, **51**, 1153-1158.
23. Q. Peng, Y. L. Niu, Q. H. Shi, X. Gao and Z. G. Shuai, *J. Chem. Theory Comput.*, 2013, **9**, 1132-1143.
24. Z. G. Shuai, *Chin. J. Chem.*, 2020, **38**, 1223-1232.
25. Y. L. Niu, W. Q. Li, Q. Peng, H. Geng, Y. P. Yi, L. J. Wang, G. J. Nan, D. Wang and Z. G. Shuai, *Mol. Phys.*, 2018, **116**, 1078-1090.
26. Z. G. Shuai and Q. Peng, *Phys. Rep.-Rev. Sec. Phys. Lett.*, 2014, **537**, 123-156.
27. Z. G. Shuai and Q. Peng, *Natl. Sci. Rev.*, 2017, **4**, 224-239.
28. Y. Niu, Q. Peng, C. Deng, X. Gao and Z. Shuai, *J. Phys. Chem. A*, 2010, **114**, 7817-7831.